In vivo bioimpedance changes during haemorrhagic and ischaemic stroke in rats: towards 3D stroke imaging using electrical impedance tomography

You may also be interested in:

Are patient specific meshes required for EIT head imaging?
Markus Jehl, Kirill Aristovich, Mayo Faulkner et al.

An electrode addressing protocol for imaging brain function with electrical impedance tomography
L Fabrizi, A McEwan, T Oh et al.

Design and calibration of a compact multi-frequency EIT system for acute stroke imaging
A McEwan, A Romsauerova, R Yerworth et al.

Use of statistical parametric mapping (SPM) to enhance electrical impedance tomography (EIT) image sets
R J Yerworth, Y Zhang, T Tidswell et al.

A comparison of two EIT systems suitable for imaging impedance changes in epilepsy
L Fabrizi, A McEwan, T Oh et al.

Stroke type differentiation using spectrally constrained multifrequency EIT: evaluation of feasibility in a realistic head model
Emma Malone, Markus Jehl, Simon Arridge et al.

In vivo bioimpedance changes during haemorrhagic and ischaemic stroke in rats: towards 3D stroke imaging using electrical impedance tomography

T Dowrick, C Blochet and D Holder

Department of Medical Physics & Biomedical Engineering, University College London, London, UK

E-mail: t.dowrick@ucl.ac.uk

Abstract

Electrical impedance tomography (EIT) could be used as a portable non-invasive means to image the development of ischaemic stroke or haemorrhage. The purpose of this study was to examine if this was possible using time difference imaging, in the anesthetised rat using 40 spring-loaded scalp electrodes with applied constant currents of 50–150 μA at 2 kHz. Impedance changes in the largest 10% of electrode combinations were $-12.8\% \pm 12.0\%$ over the first 10 min for haemorrhage and $+46.1\% \pm 37.2\%$ over one hour for ischaemic stroke (mean $\pm$ SD, $n = 7$ in each group). The volume of the pathologies, assessed by tissue section and histology post-mortem, was 12.6 μl $\pm$ 17.6 μl and 12.6 μl $\pm$ 17.6 μl for haemorrhage and ischaemia respectively. In time difference EIT images, there was a correspondence with the pathology in 3/7 cases of haemorrhage and none of the ischaemic strokes. Although the net impedance changes were physiologically reasonable and consistent with expectations from the literature, it was disappointing that it was not possible to obtain reliable EIT images. The reason for this are not clear, but probably include confounding effects of secondary ischaemia for haemorrhage and tissue and cerebrospinal fluid shifts for the stroke model. With this method, it does not appear that EIT with scalp electrodes is yet ready for clinical use.

Keywords: electrical impedance tomography, stroke, haemorrhage, ischaemia, rat model

(Some figures may appear in colour only in the online journal)

1. Introduction

The ability to rapidly differentiate haemorrhagic and ischaemic stroke, to enable appropriate treatment, is one of the most important challenges in stroke management and care (Donnan *et al* 2009). Thrombolytic 'clot-busting' drugs are a treatment for acute ischaemic stroke which must be administered within four and a half hours after the onset of symptoms (Hacke *et al* 2008). To enable effective treatment within this restricted time window, new methods are required to distinguish haemorrhagic from ischaemic stroke, without waiting for hospital admission and a computed tomography (CT) or magnetic resonance imaging (MRI) scan. It is estimated that in most countries, only 4%–10% of potentially eligible patients receive the treatment (Bambauer *et al* 2006, Innocenti *et al* 2014), primarily because of delayed admission to stroke centres. Electrical impedance tomography (EIT) has the potential to provide an inexpensive portable unit for use in ambulances or GP surgeries which would revolutionise thrombolytic management of stroke by providing imaging at the point of contact. A first step to achieving this goal is to confirm the ability of EIT to distinguish between haemorrhagic and ischaemic stroke using time difference imaging, before more advanced methods, such as frequency difference imaging (Malone *et al* 2014) are attempted.

1.1. Introduction to EIT

EIT is a safe, portable and inexpensive imaging method, where insensible electrical currents are injected into an object at a frequency between several kHz and several MHz. EIT has the potential to image brain function and pathology, with current applications including localization of epileptic foci (Bagshaw *et al* 2003, Fabrizi *et al* 2006), imaging normal haemodynamic brain function (Tidswell *et al* 2001) and fast neural activity (Boone and Holder 1995, Aristovich *et al* 2016). We have previously undertaken work to measure *in vivo* the impedance of healthy brain, ischaemic brain and blood. The study showed a clear distinction between the three impedances ($\Omega_{blood} < \Omega_{brain} < \Omega_{ischaemia}$), reinforcing the idea that EIT can successfully distinguish ischaemic from haemorrhagic stroke (Dowrick *et al* 2015).

A number of reconstruction algorithms have been proposed for the imaging of stroke, including time, frequency (Malone *et al* 2014) and absolute imaging methods (Ma *et al* 2014). Of these, frequency difference is the most promising for a clinical setting, as it allows image construction to take place using data collected at a single point in time, whereas time difference algorithms require a 'baseline' data set, recorded before the stroke onset. However, frequency difference imaging presents a substantially greater technical challenge, and is not yet implemented for *in vivo* use, as image reconstruction currently takes several hours. In contrast, time difference imaging is available and well characterised; it could provide images of the development of ischaemic stroke of haemorrhage over time in conditions for monitoring after head injury, subarachnoid haemorrhage or the evolution of stroke after thrombolytic therapy. Its application to imaging in an animal model is the basis of this work.

1.2. Literature review—impedance of brain and blood, stroke imaging using EIT

The resistivity of grey matter is 30 Ω m^{-1} at DC, decreasing to 10 Ω m^{-1} at 1 kHz and 7.5 Ω m^{-1} at 100 kHz (Gabriel *et al* 1996). The impedance of ischaemia tissue is up to 2.5 times higher than healthy tissue at DC (Casas *et al* 1999), with the resistivity of ischaemic brain 75 Ω m^{-1} 25 Ω m^{-1} at DC and 1 kHz respectively. The resistivity of blood (1.4 Ω m^{-1}) remains constant from DC up to several MHz. In practice, the recorded impedance change at the brain surface/scalp will be attenuated by healthy brain tissue and the skull. When using scalp electrodes, the magnitude of the impedance will be 10–100 times smaller (Romsauerova *et al* 2006).

The majority of work on EIT of stroke has been carried out in animal models. Xu *et al* (2010) undertook EIT imaging of ICH using autologous blood injections in a piglet model, reconstructing images using a filtered back-projection algorithm. They successfully imaged real-time impedance changes in 2D, using electrodes placed directly on the brain. Shi *et al* (2008) implemented an ischaemia model in rabbits, consisting of direct irradiation of the brain after a hole was drilled in the skull. Rapid impedance increases were recorded using a ring of electrodes placed on the skull, but image reconstruction was not possible. Images of global ischaemia have been successfully produced in a rat model, using both cortical electrodes and scalp electrodes (Holder 1992a and 1992b).

Stroke diagnosis in humans was undertaken using the UCH Mk2.5 EIT system (Romsauerova *et al* 2006, Holder *et al* 2011). Technically robust data was collected, but reconstructed images were not of sufficient quality for clinical use.

1.3. Ischaemic stroke: pathology and animal model

Ischaemic stroke represent around 80% of all strokes (Kolominsky-Rabas *et al* 2015). Human ischaemic stroke usually results from occlusion of the middle cerebral artery (MCA) (Nakano *et al* 2001). As such, animal models which occlude this artery are the most accurate. The middle cerebral artery (MCA) occlusion model using an intraluminal filament is the most widely used model of focal ischaemia in rats and mice (Macrae 2011). In this model, a flexible monofilament is introduced directly into the carotid artery and advanced until it blocks the origin of the MCA. The advantages of this method are good reproducibility, suitability for both permanent and transient ischaemia and the technically straightforward nature of the procedure, as no craniotomy is required. It was chosen as the most suitable model for this work. However, it has the limitations that it can be difficult to identify the optimal filament dimensions, and that a successful MCA occlusion can only be confirmed after the event by post-mortem histology or diffusion MRI. Infarct volumes may be quantified from histological staining. 2, 3, 5-triphenyltetrazolium chloride (TTC) staining is the most widely used technique to identify infarcted tissue. It is a marker of tissue dehydrogenase and mitochondrial dysfunction and gives good contrast as early as 3 h post infarct in rats (Liu *et al* 2009).

1.4. Haemorrhagic stroke: pathology and animal model

Intracerebral haemorrhage (ICH) accounts for roughly 20% of all cases of stroke and is associated with the highest mortality rate (Leonardo *et al* 2012). Aguilar and Brott (2011) defined 'deep' ICH within the basal ganglia and internal capsule (occurrence 35–70%), brain stem (5–10%), and cerebellum (5–10%). In contrast, 'lobar' ICH (15–30%) refers to haemorrhages located in the cortical-subcortical areas. Deep ICH accounts for about two thirds of spontaneous ICH cases and lobar ICH accounts for the remaining third. Helweg-Larsen *et al* (1984) observed the following locations of lobar haemorrhages: 14% frontal, 7% parietal, 48% temporal and 31% occipital. Two main preclinical models of haemorrhagic stroke are employed (Manaenko *et al* 2011).

The bacterial collagenase injection model entails the injection of between 0.075 and 0.4 U of a bacterial collagenase into the brain, typically into the basal ganglia or striatum. The collagenase degrades the collagen found in the basal lamina of blood vessels resulting in degraded vessels that become leaky and ultimately rupture. The bleeding profile of experimental ICH begins with bleeding approximately 10 min after injection and progresses to hematoma between 4 and 24 h later. However, the pathophysiology appears to cause cytotoxic oedema as well as haemorrhage, so that the net impedance change is dominated by cell swelling and an increase in resistance (Chen *et al* 2012). As the impedance of both clotted and unclotted blood is lower than that of brain, this is therefore of limited applicability for a model of bioimpedance of haemorrhage alone.

The autologous blood injection model is one of the most common strategies used to reproduce ICH. Blood is collected from a superficial artery, such as the lateral vein in the tail and injected stereotactically into the brain. The most common target for injection is the striatum. Approximately 50–100 μl of whole blood is injected, at a rate of 5–10 μl per minute. One drawback of the blood injection model is that secondary damage to the brain will occur due to the insertion of the needle and displacement of brain tissue during blood injection, which can cause local ischaemia around the injection site.

The blood injection model was deemed the most appropriate for this study, as it allows for the haemorrhage to be easily and quickly produced. Measurement of the size and shape of the lesion can be conducted by simple histology observation after the brain has been fixed in formalin overnight.

1.5. Purpose

This work can be considered as a feasibility study on distinguishing ischaemic and haemorrhagic stroke in a rat model using EIT, utilising recent advances in EIT hardware and image reconstruction methods. Specifically, we were interested in answering the following questions: (1) Is our current EIT system able to detect a change of impedance corresponding to haemorrhagic and ischaemic stroke? (2) Is the data suitable for image reconstruction? (3) How accurate are the reconstructed images when compared to histology?

1.6. Experimental design

Three experimental stages were devised. Firstly, EIT simulations were performed using a finite element model of the rat skull, to simulate the voltage changes which can be expected for the cases of haemorrhage and ischaemia and to verify the correct operation of the imaging algorithms. Secondly, experiments were undertaken in a non-animal model (an apple) to test the EIT hardware/software in a real life scenario. Finally, *in vivo* imaging experiments were undertaken in rats, using the most suitable models of haemorrhage and ischaemia, taken from the literature.

2. Material and methods

2.1. Animal preparation

The rats were obtained from Biological Services at University College London and were bred on site. The rats were housed in a room on a 12 h light-dark cycle with 18–20 air changes per hour and had ad libitum access to food and water. All animal work undertaken were previously approved by the UK Home Office and in accordance with the Animals (Scientific

Procedures) Act 1986 regulations and the European Directive 2010/63/EU on the protection of animals used for scientific purposes. Sprague-Dawley rats (270–430 g) were anaesthetised using Isoflurane (5% induction, 2–2.5% maintenance) in a mixture with 2:1 medical air and medical oxygen. The body temperature was controlled with a rectal probe and maintained at 36.5 °C by a heating blanket system (Harvard Apparatus, Ltd, UK). An artery line was placed in the femoral artery to monitor blood pressure and the femoral vein was also cannulated to allow intravenous access and saline injected as fluid replacement. Rats were placed in a stereotaxic frame (Narishige International Ltd, UK) in the prone position using ear bars. The rat's head was then shaved and the skin incised using a scalpel. The skull was freed from the periosteum and cleaned in order for the electrodes to be positioned directly on the skull and EIT to be recorded. A silver–silver chloride ground electrode was placed under the skin of the back of the head.

2.1.1. Intracerebral haemorrhage model. Prior to the femoral cannulation, rats were intubated and ventilated. End tidal CO_2 ($EtCO_2$) and saturation in oxygen (SpO_2) were monitored using a spirometer. Once in the stereotactic frame, a hole was drilled through the right temporal bone, 6 mm deep from the surface of the skull, 4 mm deep from the top of the skull and around Bregma. Then a 26 G (0.47 mm) cannula was inserted horizontally. Autologous blood for the ICH was collected from the femoral artery line. The blood was injected via the cannula inserted in the skull, 50 μl of whole blood was injected at a rate of 5 μl per minute. Upon completion of the experiment, the rat was humanely culled by overdose of anaesthetics. The haemorrhagic brain was taken out and immersed in formalin overnight. The brain was then coronally sliced at the injection point in order to measure the size and volume of the haemorrhage. A CT scan of the rat's skull was performed to allow for generation of custom meshes for each experiment if required. Seven experiments in total were performed.

2.1.2. Ischaemic model. Anaesthesia was induced and the rat prepared as described for the haemorrhage experiments. After the femoral cannulation, both carotid arteries were isolated and a silicon rubber-coated monofilament of 0.35 mm coated diameter (Doccol Corporation, Redlands, CA) was inserted in the right carotid artery just before it occludes the MCA. Then the rat was placed in the stereotactic frame, electrodes positioned on the rat's skull and a baseline was recorded. The filament was then pushed up until it blocked the MCA and the contralateral artery was occluded using a microvascular clip. In order for successful TTC staining following the procedure, the length of the experiment was set to 4 h. In three cases, it was not possible to record data at the 3 h mark due to technical difficulties. In a further two cases, data collection at the 4 h mark was not possible. After data acquisition, the rat was humanely culled by overdose of anaesthetics. The ischaemic brain was taken out and a TTC staining was performed. Again, seven experiments were performed and CT scans of the skull carried out on conclusion of the experiment and histology. A further seven experiments were undertaken, but were excluded from the final analysis as no ischaemia was present in the histology.

2.2. EIT: hardware—electrodes—protocols

Data were collected using a custom EIT system (Dowrick *et al* 2014) consisting of a Keithley 6221 current source (Keithley Instruments Inc., USA) combined with a BioSemi EEG system for parallel voltage measurements(ActiveTwo, BioSemi, Netherlands). 40 spring-loaded gold-plated electrodes, with a 1 mm^2 contact area, placed in a 3D printed helmet, adjustable on the stereotactic frame, were placed on the rat skull (figure 1). To increase the number of possible measurements, a silver-silver chloride electrode, used only for current injection,
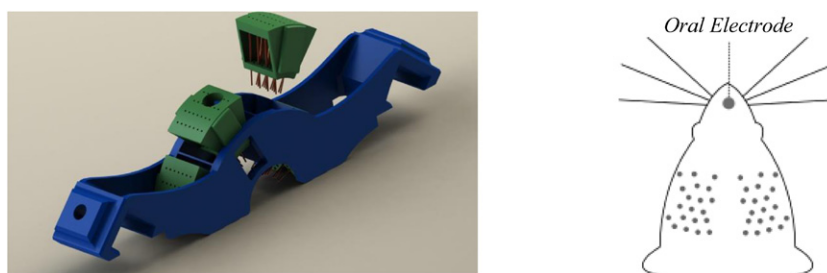
Figure 1. 3D printed electrode helmet and diagram showing electrode locations on rat skull. The helmet consists of 4 electrode modules, which can be independently adjusted, while also providing access to the rat skull in order to carry out the haemorrhage procedure.

was inserted in the mouth of the rat and a ground electrode was placed under the skin at the base of the neck. Current was injected between the left and right banks of electrodes and between the electrode in the animal's mouth and the cranial electrodes. A constant current of between 50 and 150 μA at 2 kHz was injected through up to 60 pairs of electrodes; voltages from all other electrodes were collected with reference to the ground electrode. The protocol was slightly modified for each experiment as channels which exhibited contact impedance greater than 10 kΩ were discarded based on visual inspection of the data before data collection. The mean number of electrodes excluded per experiment was 3 (minimum 1, maximum 7). Each current injection lasted 1 s, allowing a full set of measurements (a single frame of data) to be collected in under a minute. Baseline EIT data was recorded for 10–20 min at the start of the experiment, after which the perturbation was triggered. For the haemorrhage experiment, frames of data were recorded continuously, for up to 20 min after blood injection commenced. For ischaemia experiments, a frame was collected every five minutes during the first 1–2 h, where the largest and most rapid impedance changes were expected, then at thirty minute intervals over the remaining three hours.

2.3. Data processing methods simulation and image reconstruction

Recorded data was bandpass filtered (5th order Butterworth) with a bandwidth of $\pm$50 Hz around the injection frequency (2 kHz), demodulated and then averaged across each 1s injection period, to produce an array of voltage measurements for each recorded frame. During demodulation, only the resistive (real) component of the signal was considered, with the reactive (imaginary) component discarded. At 2 kHz, the phase shift in the measured signal is less than 0.5° (Dowrick *et al* 2015), as such the reactive component of the signal can be considered negligible. Voltage measurements were converted to voltage difference data by subtracting the baseline data set. Cleaning criteria were established to remove 'bad' or noisy measurements, caused by contact impedance drift, or by the shifting of electrode positions over the course of the experiments. Noisy/artefactual measurements were excluded from the data set if (a) the standard deviation during the injection period was more than 5% of the mean value or (b) the relative voltage change was greater than 200% (typical changes are expected to be in the order of 10%). Less than 10% of measurements were excluded based on these criteria. Simulations were carried out to estimate the impedance and voltage changes caused by a haemorrhage with volume 50 μl, injected over 10 min, and ischaemic event affecting the entire right hemisphere, over four hours. In both cases, a linear perturbation growth over time was simulated and appropriate impedance values for each tissue type were used. To give an indication of the

relative impedance changes for each experiment, the average of the largest 10% (in absolute terms) of impedance changes was calculated. This approach was preferred to simply taking the average of all changes, as it is more indicative of the magnitude of impedance changes caused by changes to the physiology. If the average of all channels is taken, the underlying trends remain the same, but the values are much smaller due to the large number of measurements which are unaffected by the physiological changes. The images were reconstructed using a linear approximation and inversion of a sensitivity matrix with zeroth-order Tikhonov regularisation, and a 4 million element, finite element mesh of a generic rat skull, obtained from CT scans (Aristovich *et al* 2014). A noise based correction, which converts impedance changes to significance values, was used following Tikhonov regularisation. Further details of the simulation, imaging and noise correction algorithms are given in appendix. In a single instance (Haemorrhage Rat 6), a custom mesh of the rat skull was generated from CT scans, to allow for comparison of image quality with those produced using a generic mesh.

Final 2D slices and 3D images were rendered using ParaView, with the colour scale normalised based on the significance values from the noise correction algorithm. For 3D images, it was desirable that only the largest impedance changes were visible, so a half-maximum threshold was applied to the data.

Criteria were established for assessing the quality of the reconstructed images. (1) Are the reconstructed impedance changes of the correct direction (increase for ischaemia, decrease for haemorrhage)? (2) Is the location of the reconstruction correct, where correct is defined as occurring in the same octant of the brain as the perturbation? (3) To what extent is the image affected by artefact? This was assessed by comparing the volume of the reconstructed perturbation, with the total volume of artefacts in the final 3D images.

2.4. System evaluation

In order to confirm correct operation of the EIT system and the imaging algorithms in less complex imaging scenario prior to undertaking animal experiments, EIT data was collected on an apple, with diameter 6 cm, using the same electrode arrangement and hardware as for the animal experiments. Data was collected before and after the insertion of a metal rod, 1 cm in diameter, which had a higher conductivity than the apple. The rod was inserted 1 cm deep at two locations, at the centre of the electrode array on either side of the helmet, with five frames of data collected before and after insertion in each case. Images were reconstructed using a spherical mesh.

3. Results

3.1. System test—imaging impedance changes in an apple

A decrease in the recorded voltages (5.4 mV $\pm$ 5.6 mV) and impedance changes (16.0% $\pm$ 19.9%), following the insertion of the metal rod was observed. Figures are given as mean $\pm$ SD. Reconstructed images matched the known location of the perturbation, with no image artefact present outside of the perturbation region, with the half-maximum threshold applied (figure 2).

3.2. Histology

Although a fixed volume of 50 μl of blood was injected to create each haemorrhage, there was considerable variation in the size and shape of the formed haemorrhage, presumably
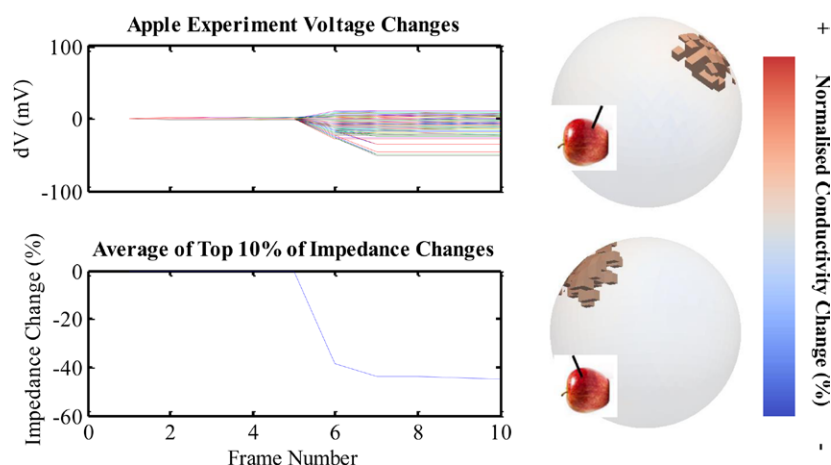
Figure 2. Voltage and impedance data for apple measurements for a single position of metal rod. The reconstructed images for both positions are shown, with insets indicating the true position.
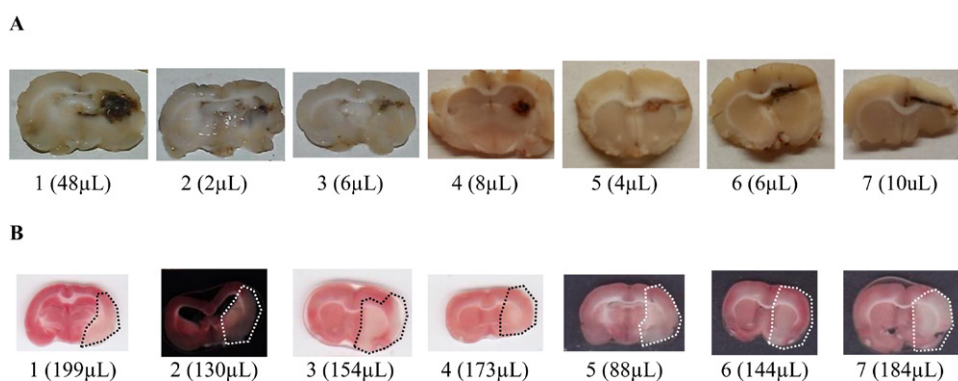

Figure 3. Coronal brain slices showing haemorrhage/ischaemia. The volume of the haemorrhage, estimated from measurements taken across multiple slices, is indicated. Ischaemia tissue is coloured white-light pink by the staining process. (A) Haemorrhage. (B) Ischaemia.

because some injected blood was absorbed or leaked away. The largest extents and volumes of the resulting, often irregular pathological regions were 2.7 mm $\pm$ 1.7 mm (1 mm–5 mm) and 12.6 μl $\pm$ 17.6 μl (2 μl–48 μl) respectively (figure 3(A)).

For ischaemia (figure 3(B)), the healthy cerebral tissue is coloured in pink–red while the ischaemic tissue remains white–light pink. The volume of ischaemic tissue, 153 μl $\pm$ 37 μl (88 μl–199 μl), was estimated from the histology by measuring the regions of tissue discoloured by the staining procedure.

3.3. Voltage and impedance changes

For the haemorrhage experiments, voltage changes of 200 μV $\pm$ 51 μV occurred before blood injection. Subsequently, changes of 20.6 mV $\pm$ 5.4 mV occurred over the 10 min injection, with a further increase of 2.2 mV $\pm$ 1.4 mV over the remaining measurement time. The simulated
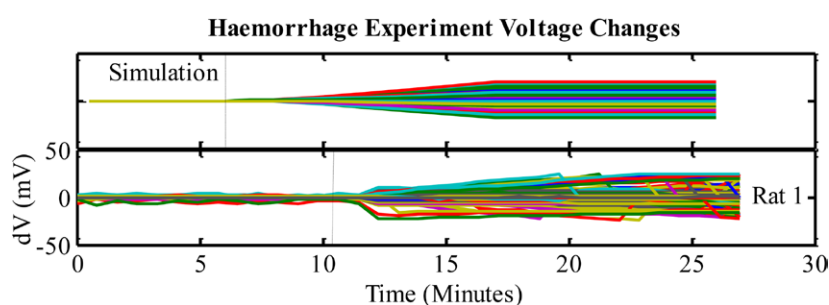
Figure 4. Voltage changes, relative to a baseline recording, during haemorrhage simulation and experiment. The dotted line indicates the start of blood injection, which took place over 10 min.
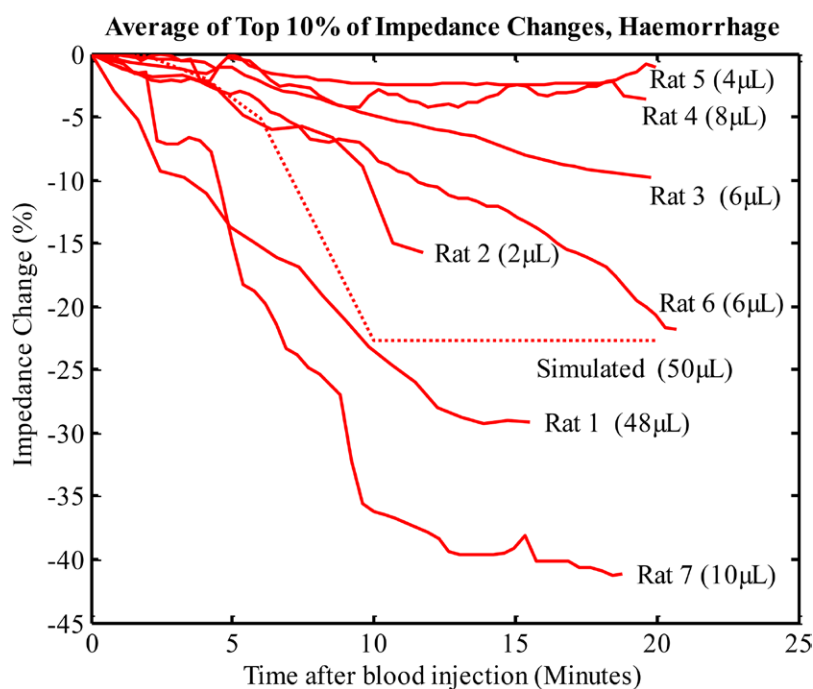

Figure 5. Average impedance change during haemorrhage experiments, with haemorrhage volume.

voltage (figure 4) and impedance changes had maximum values of 10 mV and -22.3% in simulated and experimental cases, impedance changes in both the positive and negative directions were observed, but the net change in both cases was negative, as expected for haemorrhage. The largest 10% of impedance changes (figure 5) were $-12.8\% \pm 12.0\%$ over the first 10 min and $-4.3\% \pm 3.8\%$ in the remaining time. The time course of these changes is consistent with blood injection occurring over the first 10 min. For ischaemia experiments, impedance changes occurred shortly after occlusion of the MCA, with the largest changes occurring during the first 1–2 h (figure 6). In two out of the seven (rats 4 and 6) cases, the recorded changes occurred within the first 15 min. Maximum voltage changes were 66.2 mV $\pm$ 25.0 mV during the first hour and 13.6 mV $\pm$ 12.1 mV over the remaining time. The corresponding changes in
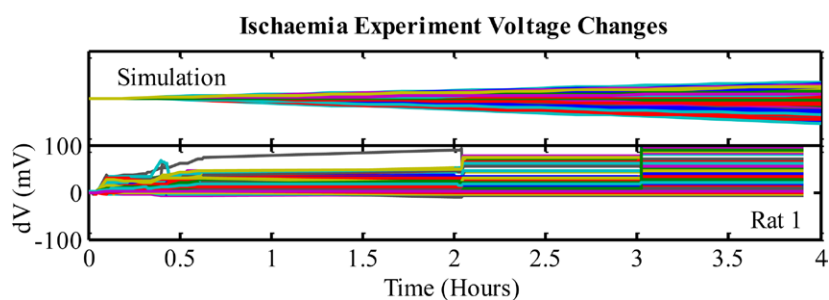
Ischaemia Experiment Voltage Changes

Figure 6. Voltage changes, relative to a baseline recording, during ischaemia simulations and experiment. Data was recorded every 5 min during the first two hours, then every half hour thereafter.
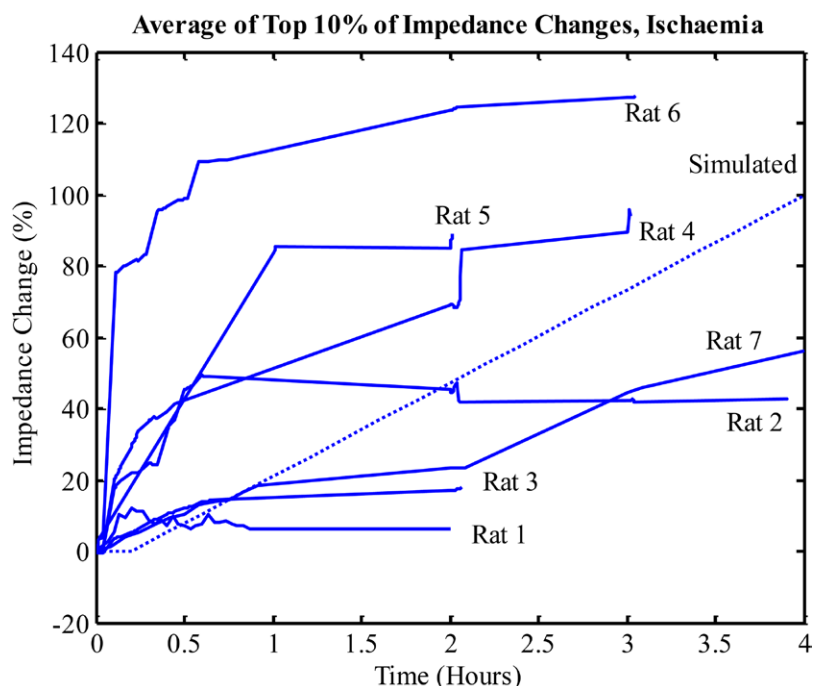

Figure 7. Average impedance during ischaemia experiments.

the top 10% of values (figure 7) were 46.1 ± 37.2% and 14.4% ± 18.7%. Maximum values of simulated data were 50 mV and 100%.

3.4. Reconstructed images

Using simulated data (figures 8 and 9), the reconstruction process successfully reproduced the location of the perturbations. For haemorrhage (figure 10), in three out of the seven experiments (1, 3 and 7), the location (but not the shape) of the haemorrhage corresponded to the location seen in the pathology. In rat 4, the locations matched but there was substantial surrounding artefact. The remaining three sets of data did not result in accurate images. As EIT
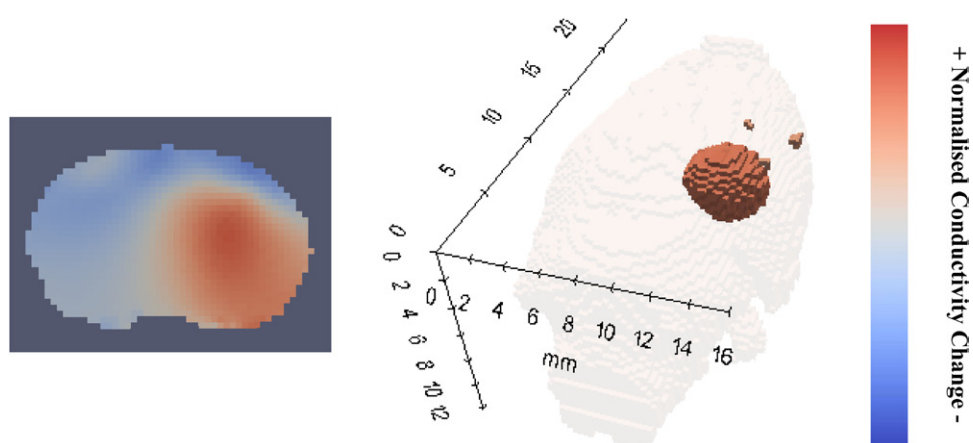
Figure 8. Image reconstruction of simulated haemorrhage data. 2D slice taken at the centre of the haemorrhage. All units in mm. For the 3D image, data was thresholded at full-width half-maximum. Red indicates increased conductivity, which is expected for haemorrhage.
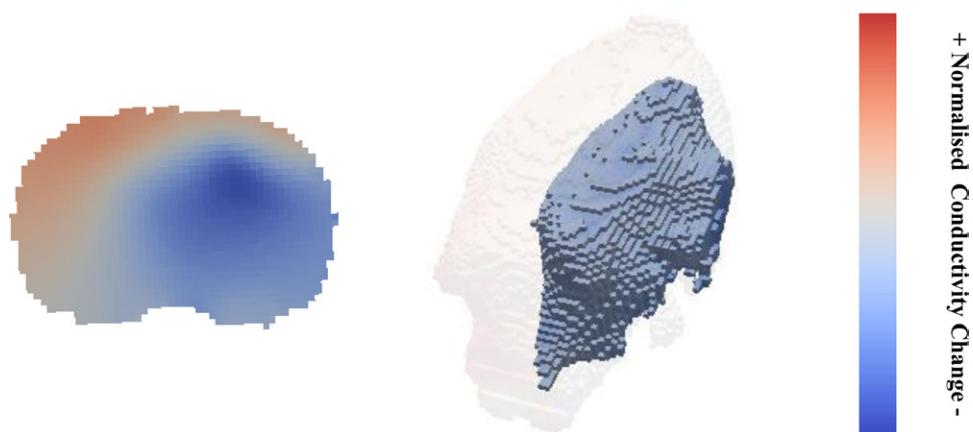

Figure 9. Image reconstruction of simulated ischaemia data. 2D slice taken at the centre of the ischaemia. Blue indicates decreased conductivity, which is expected for ischaemic brain.

data was acquired continuously during the experiment, images were reconstructed at each time step, showing the growth of the haemorrhage in the brain (figures 11 and 12), over 15 and 20 min respectively. Haemorrhage growth becomes visible in the reconstructions at 5 min and 6 min, with increases in size seen each minute, until the 12 and 8 min marks, after which the size remains stable. A custom mesh, generated from a CT scan, was created for rat 6 and the reconstructed images compared with those produced using a generic mesh (figure 13), but there was no significant difference in image quality.

For the ischaemia data, (figure 14), while the reconstructed impedance changes appeared on the same side of the brain as the ischaemia, with the exception of rat 2, they were discontinuous and a large amount of artefact was present. As such, none of the image changes corresponded to the known pathology.
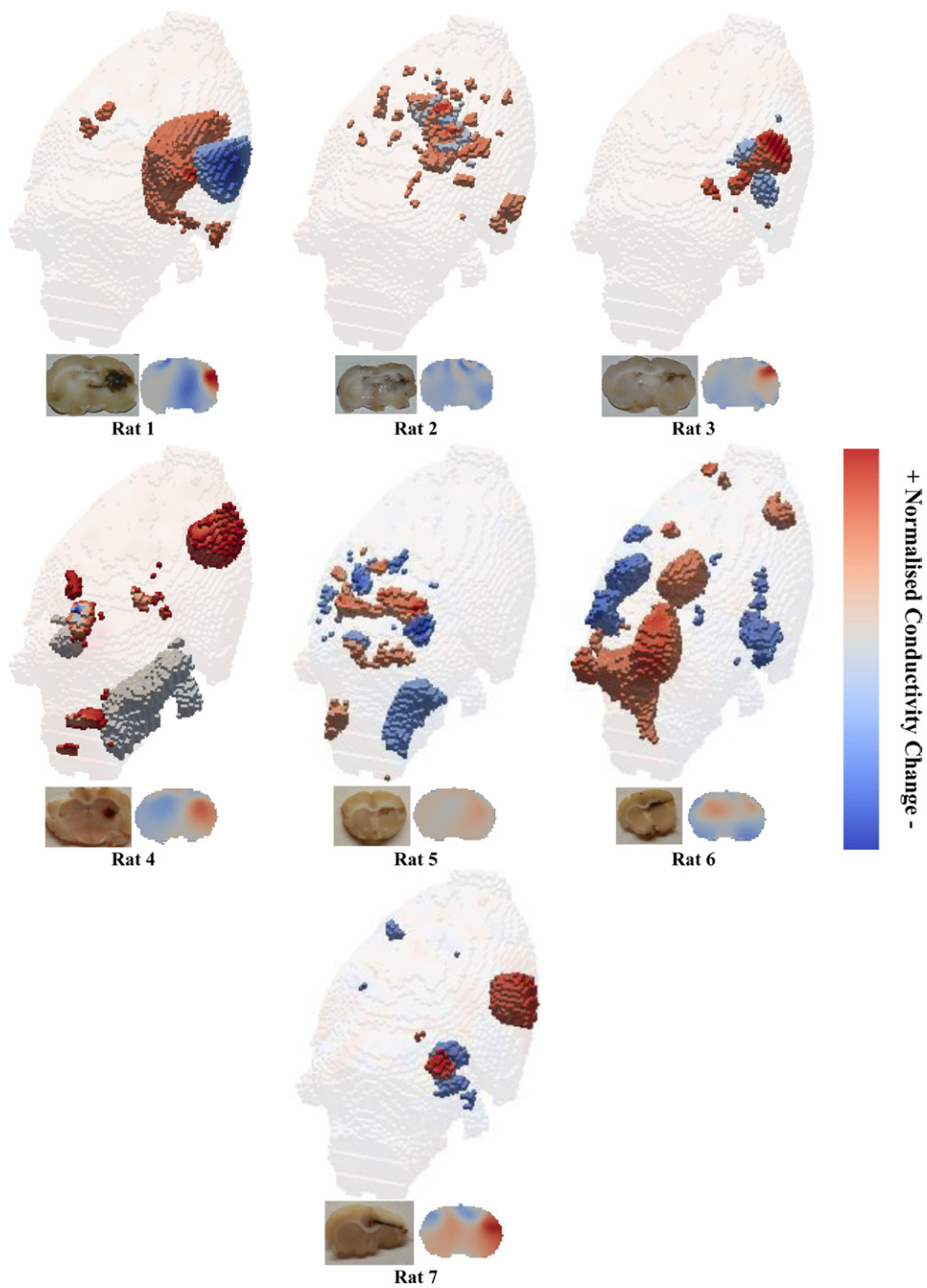
Figure 10. Image reconstruction of experimental haemorrhage data. 2D slice taken at the location of the blood injection. The location of the haemorrhage corresponded to the known pathology in rats 1, 3, 4 and 7.
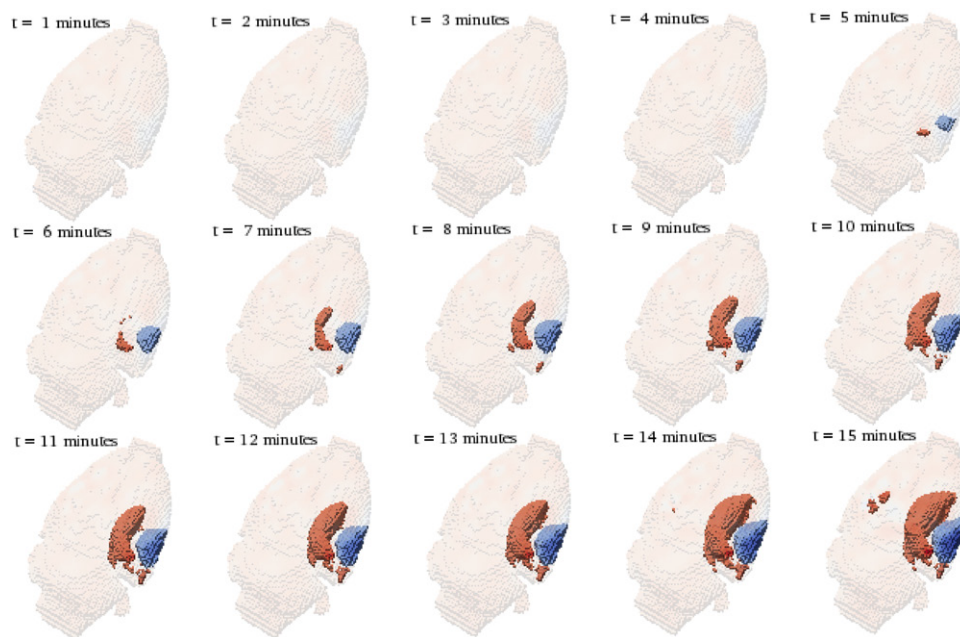
Figure 11. Reconstructions over time for Rat 1 (Haemorrhage).

There was a correlation between the size of the haemorrhage formed and the quality of the reconstructed images; the lowest quality images occurred with blood volumes under 5 μl (table 1).

4. Discussion

4.1. Summary of work

This work constitutes the first reported impedance recordings over time of haemorrhagic and ischaemic stroke using an *in vivo* rat model, where the same experimental setup was used for both sets of recordings. The recorded impedance changes, in 14 rats, were consistent with the existing literature on the subject, simulations and the known pathology. In all cases, recorded impedance changes were negative for haemorrhage, with a time course of 10–20 min, (figure 5), and positive for ischaemia, with a time course of 1–3 h (figure 7). Reconstructed images, in three out of seven cases of haemorrhage, accurately reproduced the haemorrhage location with minimal artefact. No accurate images were produced in the ischaemia cases.

4.2. Technical performance and limitations

4.2.1. Impedance changes and data quality.   The technical specifications of the EIT hardware has previously been reported (Dowrick *et al* 2014). The experimental data was of good quality, with approximately 10% of data being excluded based on the cleaning criteria set out in section 2.3. The impedance changes measured were as expected (decrease for haemorrhage, increase for ischaemia), with a time course consistent with the underlying physiological changes, and the magnitude in good agreement with the material previously published and simulated data. Good stability was seen in the baseline measurements, with the mean value of voltage fluctuations less than 0.2 mV, which is negligible (<1%) compared to the observed changes.
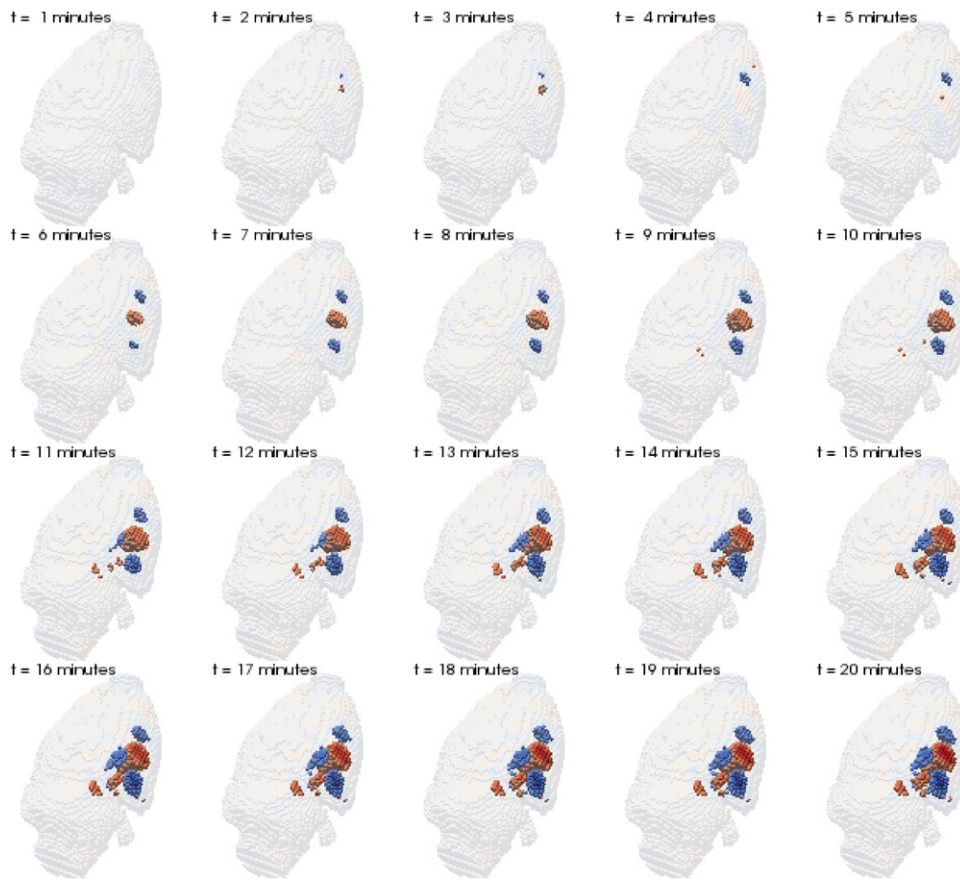
Figure 12. Reconstructions over time for Rat 3 (Haemorrhage).

Generic mesh   Custom mesh

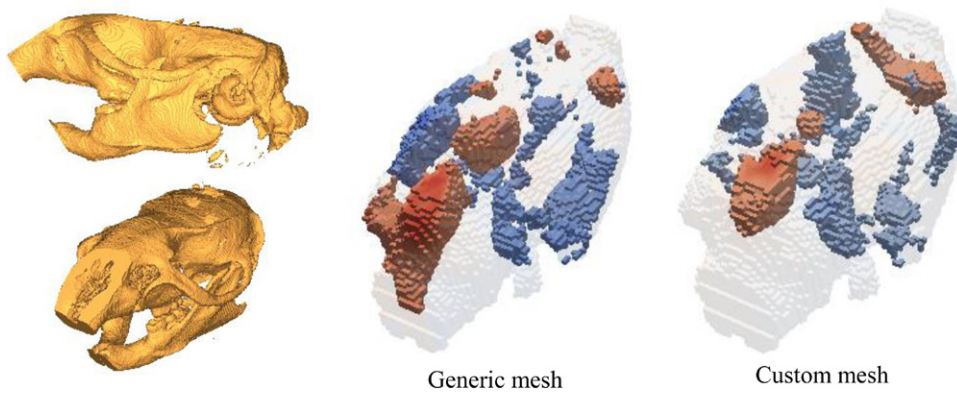**Figure 13.** Rat skull model generated from CT scan (left). Reconstructions of data from rat 6 (haemorrhage) using generic (middle) and custom (right) meshes. The use of the custom mesh didnot result in a more accurate localisation of the haemorrhage, or a reduction in artefact.
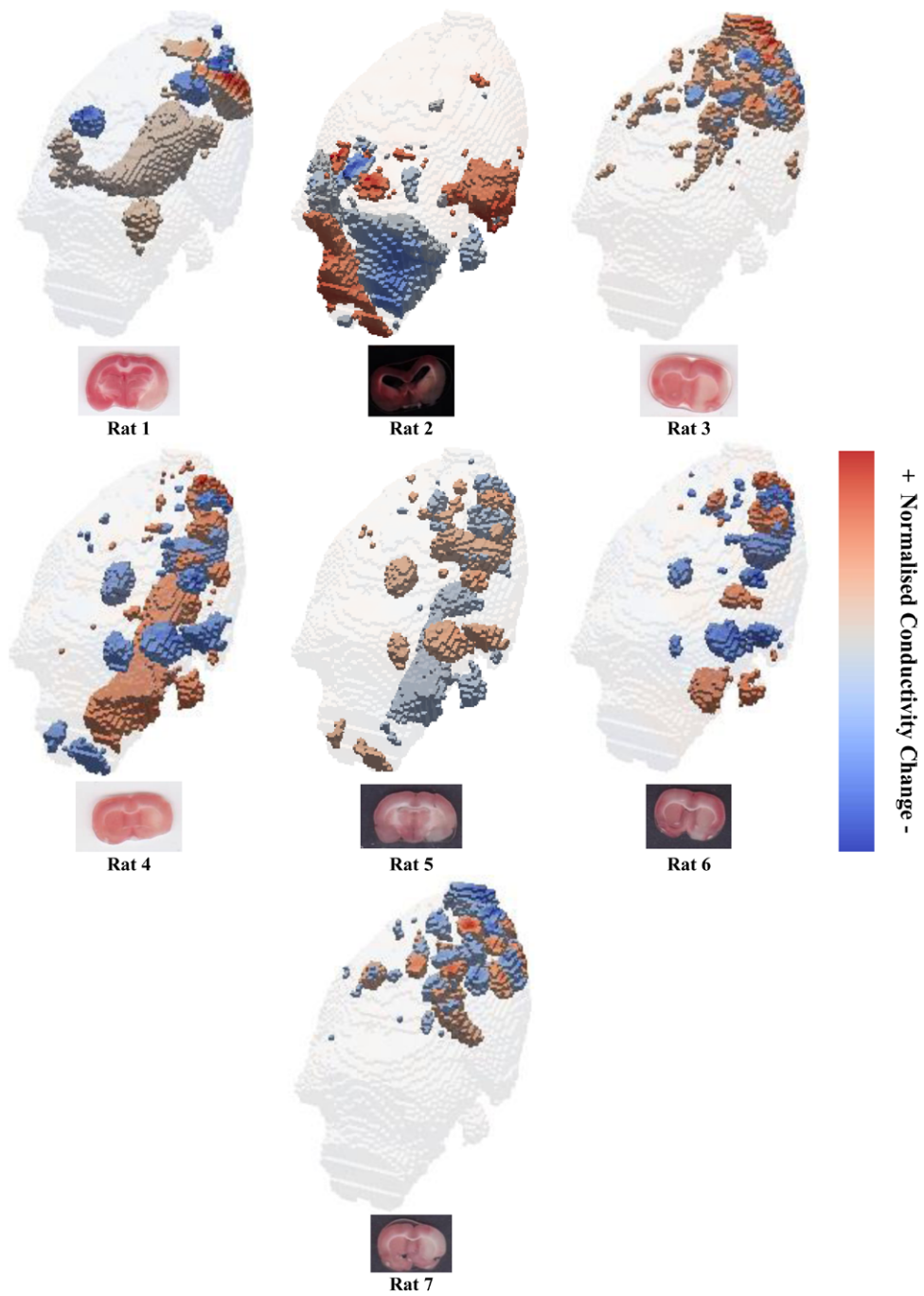
Figure 14. Image reconstruction of experimental ischaemia data. Large amounts of artefact are present in all images.

Table 1. Summary of image accuracy.

Rat	Haemorrhage (estimated blood volume)							Ischaemia						
	1 (52 μl)	2 (2 μl)	3 (6 μl)	4 (8 μl)	5 (4 μl)	6 (6 μl)	7 (10 μl)	1	2	3	4	5	6	7
Direction of change	✓	✗	✓	✓	✗	✓	✓	✗	✗	✗	✗	✗	✗	✗
Location	✓	✗	✓	✓	✗	✗	✓	✓	✗	✓	✓	✓	✓	✓
Minimal artefacts	✓	✗	✓	✗	✗	✗	✓	✗	✗	✗	✗	✗	✗	✗
Overall	✓	✗	✓	✓/✗	✗	✗	✓	✗	✗	✗	✗	✗	✗	✗

4.2.2. Limitations of the animal models. The haemorrhagic animal model used is one of the most common (Manaenko *et al* 2011), but the need to drill a hole in the skull and to insert a cannula in the brain to inject blood is far removed from the physiological physiology of haemorrhagic stroke. Large variations in the size and shape of the clotted blood occurred (figure 3(A)). Backflow of blood along the needle track and blood clotting in the tubing required for the injection were identified as prominent causes of the reduced blood volume. Additionally, it is thought that some blood diffuses in the brain before clotting, explaining the non-spherical shape of several of the blood clots. It is also expected that some local ischaemia may be caused around the site of the blood injection, due to damage associated with the surgical procedure, which may manifest as an impedance increase around the haemorrhage site.

4.2.3. Non-homogenous impedance changes. As previously discussed, the physiological processes underlying both the haemorrhage and ischaemia cases can cause non-homogenous impedance changes, which are not predicted by simulations or the model, introducing artefacts into the images. This is made more problematic by the lack of any simultaneous, independent, measurements to validate the experimental changes. While histology is a useful tool for assessing image accuracy, particularly for the haemorrhage experiments, it only provides information on the state of the brain after the experiment has been concluded, it does not provide any information as to the physiological changes at the time data was collected. This was especially an issue for the ischaemia experiments, where the impedance changes occurring throughout the hemisphere may have occurred in a non-uniform and non-linear fashion. Ideally, simultaneous MRI data would be collected alongside the EIT data, to provide a gold standard set of images for comparison.

4.3. Image quality

Some artefact was present in all of the images, particularly for the ischaemia experiments. These may be sub-divided into physiological artefact, where there is some impedance change apart from the expected change, or where the impedance change in non-homogenous; and artefact due to noise in the data and/or the reconstruction algorithm. For the haemorrhage experiments, possible sources of physiological artefact include tissue damage caused by the cannula used for blood injection, and local ischaemia around the injection site as the blood volume increases. In future, varying the rate of blood injection between experiments may allow for greater discrimination between the expected impedance changes due to the injection and physiological artefacts. For the ischaemic case, the model, and simulations assume that there is a strictly linear increase in tissue impedance across time, when in reality different portions of the brain may be affected to different degrees, over different time periods.

4.4. Conclusions

This work has provided an insight into the challenges faced for the imaging of stroke using EIT. *In vivo* EIT data has been collected using scalp electrodes on 14 rats, during intracerebral haemorrhage and ischaemia. Impedance changes, consistent with the underlying physiological changes have been recorded. The overall purpose of this work was to investigate the possibility of EIT imaging of stroke, utilising recent advantages in hardware and image reconstruction techniques. In this respect, time difference images have been successfully reconstructed in some cases for haemorrhage, but not for ischaemia, and the overall quality of images is not yet of sufficient quality to be determined a success.

4.4.1. Implications for clinical use.   The main purpose of this work was to investigate the use of EIT for the diagnosis and differentiation of haemorrhagic and ischaemic stroke. The overall quality of images was not sufficiently high to be considered successful, or to justify human experiments, but a number of observations can be drawn.

The imaging of haemorrhage has been, in some cases, successful, with some correlation between the size of the haemorrhage and the quality of the image. It may be that there is some minimum size of clot that can be detected using EIT, which is an area that should be investigated further.

Even though the images were not in all cases accurate, the measured impedance data (figures 5 and 7) are consistent with the underlying physiological changes. For the purposes of diagnosis, it may be possible to use a machine learning approach to classify the data (Aristovich *et al* 2015).

4.4.2. Future work.   A number of potential improvements to the experimental setup have been proposed, and future work will include improvements to the animal model to more closely mirror the real life cases, more accurate simulations to study the cases where haemorrhage and ischaemia may occur at the same time and simultaneous imaging using MRI/CT to provide an independent set of data for comparison.

Acknowledgments

Appendix. Simulation and imaging algorithms

A.1. Simulations

An anatomically realistic model of the rat skull and brain, obtained from an MRI image, was used, with electrode positions matching those used experimentally. The w of the skull, cerebrospinal fluid and grey matter were constant and isotropic (0.018, 1.79 and 0.3 Sm^{-1} respectively). The simulated perturbation for haemorrhage was a sphere of blood (conductivity 0.9 Sm^{-1}) linearly increasing in volume to 50 μl. For ischaemia, the conductivity of the entire right hemisphere was linearly reduced to 0.15 Sm^{-1}, to model the decreased impedance of ischaemic tissue.

A.2. Forward solution

The forward solution is computed by solving the quasistatic Maxwell equation in space, with the complete electrode model boundary conditions for pairs of electrodes:

$$\nabla \cdot \sigma \nabla u = 0$$

$$\sigma \frac{\partial u}{\partial n} = 0 \text{ off } \bigcup_{i=1}^{2} e_i$$

$$u + z_i \sigma \frac{\partial u}{\partial n} = V_i \ i = 1, 2 \tag{A.1}$$

Where u is the electric potential, σ is the conductivity, n is the normal to the boundary, e_1 is the lth electrode boundary, z_i is the contact impedance in the ith electrode and V_i is the measured voltage. For each injection pair, the voltages at all other electrodes were calculated, and the process was repeated for each injection pair. Using an assumption of linearity of the measured voltage changes with respect to the conductivity change in the volume, it was possible to construct a Jacobian matrix J, which mapped the changes in conductivity in each element to changes in electrode voltages:

$$\delta u = J \delta \sigma \tag{A.2}$$

The solution of (A.1) was calculated using a finite element method and parallel forward solver (Jehl *et al* 2014)

A.3. Inverse solution

The inverse solution is calculated by inversion of J in order to obtain a linear map between the electrode voltages and conductivity changes within the mesh. As J is ill-conditioned, Zeroth-order Tikhonov regulariation is employed, using minimisation of the l2 norm:

$$\widehat{\delta\sigma} = \arg \min_{\delta\sigma} \|\delta v - J\delta\sigma\|^2 + \lambda\|\delta\sigma\|^2$$

$$J_\lambda^{-1} = (J^T J + \lambda I)^{-1} J^T \tag{A.3}$$

Where $\widehat{\delta\sigma}$ is the estimated conductivity change, δv is the voltage change and λ is a hyperparameter set using cross-validation. The optimal value of λ (chosen to minimise cross-validation error) was found using leave one out cross-validation (Picard and Cook 1984).

A.4. Noise correction algorithm

The method consists of using the inverted Jacobian matrix J_λ^{-1} in order to compute the standard deviation of the estimated conductivity change in each element of the mesh due to randon Gaussian noise in the voltage measurements ($k = 1000$ samples of the Gaussian normal distribution was taken to compute the standard deviation correctly):

$$\delta\sigma_n = J_\lambda^{-1} \delta v_n$$

$$\delta v_n \sim N(0, 0.5 \cdot 10^{-6}) \tag{A.4}$$

Here, $\delta\sigma_n$ is the conductivity change matrix of size $m \times k$ (m is the number of elements in the mesh and k is the number of voltage measurements) caused in the voltage change, δv_n on the electrodes. The z-score for the actual conductivity change in the ith element can then be computed and displayed as representative of the signal strength:

$$t_i = \frac{\delta\sigma^i}{\left\langle \delta\sigma_n^i - \overline{\delta_n^I} \right\rangle} \tag{A.5}$$

References

Aguilar I M and Brott G T 2011 Update in intracerebral hemorrhage *Neurohospitalist* **1** 148–59

Aristovich K Y, dos Santos G S, Packham B C and Holder D S 2014 A method for reconstructing tomographic images of evoked neural activity with electrical impedance tomography using intracranial planar arrays *Physiol. Meas.* **35** 1095–109

Aristovich K Y, Jehl M, Dowrick T, Blochet C and Holder D 2015 Machine learning approach to clinical stroke type differentiation using electrical impedance tomography (EIT) *Proc. of the 16th Int. Conf. on Biomedical Applications of Electrical Impedance Tomography*

Aristovich K Y, Packham B C, Koo H, dos Santos G S, McEvoy A and Holder D S 2016 Imaging fast electrical activity in the brain with electrical impedance tomography *Neuroimage* **124** 204–13

Bagshaw P A *et al* 2003 Electrical Impedance tomography of human brain function using reconstruction algorithms based on the finite element method *Neuroimage* **5** 752–64

Bambauer Z K, Johnston C, Bambauer E D and Zivin A J 2006 Reasons why few patients with acute stroke receive tissue plasminogen activator *Arch. Neurol.* **63** 661–4

Boone G K and Holder S D 1995 Design considerations and performance of a prototype system for imaging neuronal depolarization in the brain using 'direct current' electrical resistance tomography *Physiol. Meas.* **16** A87–98

Casas O, Bragós R, Riu P J, Rosell J, Tresànchez M, Warren M, Rodriguez-Sinovas A, Carreño A and Cinca J 1999 *In vivo* and *in situ* ischemic tissue characterization using electrical impedance spectroscopy *Ann. New York Acad. Sci.* **873** 51–8

Chen C, Fu F, Li B and Liu W 2012 Experimental study of detection of brain tissue with electrical impedance tomography after cerebral ischemic *Proc. of the World Congress on Medical Physics and Biomedical Engineering* pp 807–10

Donnan A G, Fisher M, Macleod M and Davis S M 2009 Stroke *Lancet* **373** 1612–23

Dowrick T, Blochet C and Holder D 2015 *In vivo* bioimpedance measurement of healthy and ischaemic rat brain: implications for stroke imaging using electrical impedance tomography *Physiol. Meas.* **36** 1273–82

Dowrick T, Blochet C, Chaulet N and Holder D 2014 A custom EIT system based on off-the-shelf equipment *Proc. of the 15th Int. Conf. on Biomedical Applications of Electrical Impedance Tomography*

Fabrizi L, Sparkes M, Horesh L, Perez-Juste Abascal J F, McEwan A, Bayford H R, Elwes R, Binnies C D and Holder S D 2006 Factors limiting the application of electrical impedance tomography for identification of regional conductivity changes using scalp electrodes during epileptic seizures in humans *Physiol. Meas.* **27** S163–74

Gabriel C, Gabriel S and Corthout E 1996 The dielectric properties of biological tissues: I. Literature survey *Phys. Med. Biol.* **41** 2231–49

Hacke W *et al* 2008 Thrombolysis with alteplase 3 to 4.5 h after acute ischemic stroke *New Engl. J. Med.* **359** 1317–29

Helweg-Larsen S, Sommer W, Strange P, Lester J and Boysen G 1984 Prognosis for patients treated conservatively for spontaneous intracerebral hematomas *Stroke* **15** 1045–8 (PMID: 6506116)

Holder S D 1992a Detection of cerebral ischaemia in the anaesthetised rat by impedance measurement with scalp electrodes: implications for non-invasive imaging stroke by electrical impedance tomorgraphy *Physiol. Meas.* **13** 63–75

Holder D S 1992b Electrical impedance tomography with cortical or scalp electrodes during global cerebral ischaemia in the anaesthetised rat *Clin. Phys. Physiol. Meas.* **13** 87–98

Holder D, Romsauerova A, Luis J and Cornell J 2011 A method for recording electrical impedance tomography images in human acute stroke subjects *Proc. of the 12th Int. Conf. on Biomedical Applications of Electrical Impedance Tomography*

Innocenti E, Nencini P, Romani I, Del Bene A, Arba F, Piccardi B and Pracucci G 2014 Delay in presentation after acute ischemic stroke: the Careggi Hospital Stroke Registry *Neurol. Sci.* **35** 49–52

Jehl M, Dedner A, Betcke T, Aristovich K, Klofkorn R and Holder D 2014 A fast parallel solver for the forward problem in electrical impedance tomography *IEEE Trans. Biomed. Eng.* **62** 126–37 (PMID: 25069109)

Kolominsky-Rabas P L, Wiedmann S, Weingartner M, Liman T G, Endres M, Schwab S, Buchfelder M and Heuschmann P U 2015 Time trends in incidence of pathological and ethiological stroke subtypes during 16 years: the Erlangen Stroke Project *Neuroepidemiology* **44** 24–9

Leonardo C C, Robbins S and Dore S 2012 Translating basic science research to clinical application: models and strategies for intracerebral hemorrhage *Frontiers Neurol.* **3** 1–14

Liu F, Schafer P D and McCullough D L 2009 TTC, fluoro-Jade B and NeuN staining confirm evolving phases of infarction induced by middle cerebral artery occlusion *J. Neurosci. Methods* **179** 1–8

Ma J, Xu C, Dai M, You F, Shi X, Dong X and Fu F 2014 Exploratory study on the methodology of fast imaging of unilateral stroke lesions by electrical impedance asymmetry in human heads *Sci. World J.* **2014** 534012

Macrae I M 2011 Preclinical stroke research—advantages and disadvantages of the most commom rodent models of focal ischemia *Br. J. Pharmacol.* **164** 1062–78

Malone E, Sato Dos Santos G, Holder D and Arridge S 2014 Multifrequency electrical impedance tomography using spectral constraints *IEEE Trans. Med. Imaging* **33** 340–50

Manaenko A, Chen H, Zhang H J and Tang J 2011 Comparison of different preclinical models of intracerebral hemorrhage *Acta Neurochir. Suppl.* **111** 9–14

Nakano S, Iseda T, Kawano H, Yoneyama T, Ikeda T and Wakisaka S 2001 Correlation of early CT signs in the deep middle cerebral artery territories with angiographically confirmed site of arterial occlusion *AJNR Am. J. Neuroradiol.* **22** 654–9

Picard R R and Cook R D 1984 Cross-validation of regression models *J. Am. Stat. Assoc.* **79** 575–83

Romsauerova A, McEwan A, Horesh L, Yerworth R, Bayford R H and Holder D S 2006 Multi-frequency electrical impedance tomography (EIT) of the adult human head: initial findings in brain tumours, arteriovenous malformations and chronic stroke, development of an analysis method and calibration *Physiol. Meas.* **27** S147

Shi X, You F, Fu F, Liu R, You Y, Dai M and Dong X 2008 Preliminary research on monitoring of cerebral ischemia using electrical impedance tomography technique *Proc. IEEE Conf. of the Eng. Med. Biol. Soc.* pp 1188–91

Tidswell A T, Gibson A, Bayford H R and Holder S D 2001 Three-dimensional electrical impedance tomography of human brain activity *Neuroimage* **13** 283–94

Xu C H *et al* 2010 Real-time imaging and detection of intracranial haemorrhage by electrical impedance tomography in a piglet model *J. Int. Med. Res.* **38** 1596–604